$LiMn_{2-x}Cu_xO_4$ Spinels ($0.1 \leq x \leq 0.5$) - A New Class of 5 V Cathode Materials for Li Batteries: I. Electrochemical, Structural and Spectroscopic Studies

by

Yair Ein-Eli*, W. F. Howard*[1], Jr. and Sharon H. Lu*
Covalent Associates, Inc.
10 State Street, Woburn, MA 01801, USA

Sanjeer Mukerjee and James McBreen*
Brookhaven National Laboratory
Upton, NY 11978-5000, USA

John T. Vaughey and Michael M. Thackeray*
Argonne National Laboratory
9700 South Cass Avenue
Argonne, IL 60439, USA

August, 1998

To be published in Vol. 496, Materials for Electrochemical Energy Storage and Conversion II - Batteries, Capacitors and Fuel Cells, Materials Research Society, Warrendale, PA.

---

*Electrochemical Society Member
[1]Current Address: Kerr-McGee Technical Center, P.O. Box 25861, Oklahoma, City, 73125-0861

DISCLAIMER

Submitted

$LiMn_{2-x}Cu_xO_4$ Spinels ($0.1 \leq x \leq 0.5$) - A new Class of 5 V Cathode Materials for Li Batteries: I. Electrochemical, Structural and Spectroscopic Studies

Yair Ein- Eli*, W. F. Howard, Jr.*[1] and Sharon H. Lu*,
Covalent Associates, Inc.,
10 State Street, Woburn, MA 01801, USA

Sanjeer Mukerjee and James McBreen*
Brookhaven National Laboratory
Upton, NY 11973-5000, USA

John T. Vaughey and Michael M. Thackeray*
Argonne National Laboratory
9700 South Cass Avenue, Argonne, IL 60439, USA

Abstract

A series of electroactive spinel compounds, $LiMn_{2-x}Cu_xO_4$ ($0.1 \leq x \leq 0.5$) has been studied by crystallographic, spectroscopic and electrochemical methods and by electron-microscopy. These $LiMn_{2-x}Cu_xO_4$ spinels are nearly identical in structure to cubic $LiMn_2O_4$ and successfully undergo reversible Li intercalation. The electrochemical data show a remarkable reversible electrochemical process at 4.9 V which is attributed to the oxidation of Cu^{2+} to Cu^{3+}. The inclusion of Cu in the spinel structure enhances the electrochemical stability of these materials upon cycling. The initial capacity of $LiMn_{2-x}Cu_xO_4$ spinels decreases with increasing x from 130 mAh/g in $LiMn_2O_4$ (x=0) to 70 mAh/g in "$LiMn_{1.5}Cu_{0.5}O_4$" (x=0.5). The data also show slight shifts to higher voltage for the delithiation reaction that normally occurs at 4.1 V in standard $Li_{1-x}Mn_2O_4$ electrodes ($1 \geq x \geq 0$) corresponding to the oxidation of Mn^{3+} to Mn^{4+}. Although the powder X-ray diffraction pattern of "$LiMn_{1.5}Cu_{0.5}O_4$" shows a single-phase spinel product, neutron diffraction data show a small, but significant quantity of an impurity phase, the composition and structure of which could not be identified. X-ray absorption spectroscopy was used to gather information about the oxidation states of the manganese and copper ions. The composition of the spinel component in the $LiMn_{1.5}Cu_{0.5}O_4$ was determined from X-ray diffraction and XANES data to be $Li_{1.01}Mn_{1.67}Cu_{0.32}O_4$ suggesting, to a best approximation, that the impurity in the sample was a lithium-copper-oxide phase. The substitution of manganese by copper enhances the reactivity of the spinel structure towards hydrogen; the compounds are more easily reduced at moderate temperature (~200 ^{0}C) than $LiMn_2O_4$.

* Electrochemical Society Member
[1] Current Address: Kerr-McGee Technical Center, P.O. Box 25861, Oklahoma City, OK, 73125-0861

Introduction

Materials that reversibly intercalate lithium form the cornerstones of the emerging lithium-ion battery industry. Lithiated graphite and pyrolyzed carbons (1,2) and more recently, glassy tin oxides (3) are the anodes of greatest interest as they offer a low potential vs. lithium, typically below 1 V. Layered rock salt compounds such as $LiCoO_2$ and $LiNiO_2$ (4,5) are proven 4 V cathode materials (6-8). Currently, $LiCoO_2$ is the preferred electrode material for commercial lithium-ion batteries (9) which are now being manufactured at a rate of 250 million units/year (10). Nonetheless, Co and Ni compounds have economic and environmental problems that leave the door open to exploit alternative materials.

The spinel $LiMn_2O_4$ is an inexpensive, environmentally benign intercalation cathode that is the subject of intense development (11), although it is not without faults. The achievable electrode capacity (120 mAh/g) is 15-30% lower than that which can be obtained from $Li(Co,Ni)O_2$ cathodes. Moreover, an unmodified $LiMn_2O_4$ electrode exhibits an unacceptably high capacity fade. Several researchers have stabilized the $LiMn_2O_4$ electrode structure to lithium insertion/extraction reactions at ~4 V by substituting a small fraction (~2.5%) of the manganese ions with other metal cations (12-14). Although these substitution techniques can successfully combat the capacity decline at 4 V, the initial reversible capacity is no better than 115 mAh/g (14).

Extending the concept of Mn replacement in the spinel, Davidson (15) and Amine (16) have used Cr and Ni, respectively, to produce $LiMn_{2-x}M_xO_4$ electrodes ($x \approx 0.5$) that provide improved stability to electrochemical cycling at 3 V. Guyomard and coworkers (17) showed that lithium extraction from the Cr-substituted spinel occurs at 4 V and 4.9 V; these reactions were

attributed to the oxidation of manganese and chromium, respectively. Gao (18) discovered that lithium extraction from $LiMn_{1.5}Ni_{0.5}O_4$ occurs at 4.7 V; they attributed this reaction to the oxidation of Ni^{2+} to Ni^{4+}.

Recently, we reported a preliminary account of the preparation and electrochemical behavior of a copper substituted spinel, $LiMn_{1.5}Cu_{0.5}O_4$ (19). In this paper, we present electrochemical, structural and spectroscopic data obtained from an examination of various compounds in the $LiMn_{2-x}Cu_xO_4$ system ($0 \leq x \leq 0.5$) which provide a much greater understanding of the behavior of these materials than initially reported (19). Structural properties and variations in the cation charge distribution are used to explain the electrochemical behavior of $LiMn_{2-x}Cu_xO_4$ electrodes. X-ray absorption studies have been used to determine the oxidation states of the manganese and copper ions. The sample, which was two-phase, consisted of a predominant spinel phase and a lithium-copper-oxide phase. The structure of the spinel component, as determined by a Rietveld refinement of the powder X-ray diffraction pattern, is presented. The influence of copper on the reactivity of the spinel structure toward hydrogen has been studied by thermogravimetric analysis.

Experimental

$LiMn_{2-x}Cu_xO_4$ ($0 \leq x \leq 0.5$) cathode materials were prepared by conventional solid state and sol-gel methods. In the solid state syntheses, $LiOH \cdot H_2O$ was intimately mixed with the required amounts of CuO and MnO_2 for a given stoichiometry, and then heated for 18 hours in air at 750° C. The product was free-flowing and did not require milling.

Nearly phase-pure $LiMn_{1.5}Cu_{0.5}O_4$ was prepared by a sol-gel process by dissolving stoichiometric amounts of CH_3COOLi (Acros), $Cu(OOCCH_3)_2 \cdot H_2O$ (Avacado), and $Mn(OOCCH_3)_2$ (Aldrich) in deionized water, and adding a 4 -times molar amount of NH_4OH. The mixture was stirred with gentle heating for 2 hours, then concentrated to dryness on a rotary evaporator. The powdered precursor was split into four samples that were treated at different temperatures, as outlined in the Discussion section that follows. Elemental analyses, undertaken by Laboratory Testing (Dublin, PA) confirmed the composition of the final materials.

Cyclic voltammograms were obtained with an EG&G/PAR potentiostat, model 263A; they were recorded at a slow sweep rate of 15 μV/s. Cycling data were collected on either a Maccor series 4000 or Starbuck multi-channel cyclers. Cathode materials were studied using a lithium foil anode (10 mil, Cyprus Foote Mineral), separated with Whatman BS-65 glass microfibers in a 1 cm^2 parallel-plate configuration. Cathode films were prepared from a slurry of $LiCu_xMn_{2-x}O_4$ with 10% PVDF (Polyvinylidene fluoride, Atochem, North America) and 10% acetylene black (w/w) dissolved in N-methyl-2-pyrrolidinone (NMP, Aldrich). The mixture was doctor-bladed onto aluminum foil, dried at 140° C under vacuum for several hours, then roll-compressed at 100 atm. Cathode discs (1 cm^2) were then punched from the sheet, with an average weight of 6 mg of active material. Cell assembly was carried out under an Ar atmosphere. The electrolyte composition was 1.2 M $LiPF_6$ (Hashimoto Chemical) in a mixture of ethylene carbonate (EC) and dimethyl carbonate (DMC) (EM Industries and Mitsubishi Chemical) in a volume ratio of 2EC:3DMC. This electrolyte was selected because of its reported stability to oxidation up to 5 V (19). Cells were charged and discharged galvanostatically at a current density of 0.25 mA/cm^2 between 3.3 and 5.1 V.

Samples were prepared for X-ray absorption spectroscopy by mixing $LiCu_{0.5}Mn_{1.5}O_4$ with BN and pressing it into a thin wafer. X-ray absorption data were collected with the storage ring operating 2.584 GeV and an electron current between 110 and 350 mA. The monochromator was operated in the two crystal mode using Si (111) crystals. The monochromator was detuned by 50% at the Mn edge and by 15% at the Cu edge to reject higher harmonics. The experiments were done in the transmission mode with three detectors. The third detector was used in conjunction with a reference sample, which was either a Cu foil or a plastic bonded Mn powder sample. In this way, the edge positions of the spectra could be calibrated. Other details of the measurements have been published (20). Since the main interest was the determination of the oxidation state of the Mn and Cu ions, only the X-ray absorption near edge fine structure (XANES) was analyzed in detail. The methods used in analyzing the XANES data are described in detail elsewhere (21). Data were also obtained on several compounds of copper and manganese with known oxidation states.

A Philips 1840 diffractometer with Fe K_α radiation was used to obtain powder X-ray diffraction patterns to characterize the samples. For the detailed structure analyses, X-ray diffraction data of two independent powder samples of $LiCu_{0.5}Mn_{1.5}O_4$ were collected on an automated Siemens D5000 diffractometer with Cu K_α radiation between 15 and 120° 2θ. The X-ray patterns of these samples showed a single-phase spinel product. By contrast, neutron diffraction data of these two samples collected by the Intense Pulsed Neutron Diffractometer (IPNS) at Argonne National Laboratory and by the High Resolution Powder Diffractometer (HRPD) at the Rutherford Laboratory (U.K.) showed evidence of a small, but significant impurity phase that could not be identified. Because of problems encountered with a two-phase

refinement of the neutron data, a best approximation of the structure of the spinel component was determined from the X-ray data by the Rietveld profile refinement technique using the software package GSAS (22).

Thermogravimetric analyses were performed by Springborn Testing & Research (Enfield, CT) using a duPont 9000 thermal analyzer equipped with a duPont 951 TGA. The samples were analyzed from 30 to 900° C at 5° C/min under hydrogen using a flow rate of 40 ml/min.

Results and Discussions

Sample Preparation

Attempts to prepare $LiMn_{2-x}Cu_xO_4$ cathode materials via conventional solid-state reaction techniques resulted in persistent MnO_x/Li_2MnO_3 impurities in the products, whereas sol-gel methods produced purer materials. The X-ray diffraction patterns of typical products (obtained with Fe K_α radiation) made by the two routes are shown in Figure 1. Three subsequent firings of the products made by the solid state reaction route reduced only marginally the Mn_2O_3/Li_2MnO_3 impurity levels. For the sol-gel route, the powdered precursor described in the Experimental section above was divided into four lots; they were heated for 18 hours in air at 350°, 500°, 650°, and 750° C, respectively. Figure 2 shows the X-ray diffraction patterns of $LiMn_{1.5}Cu_{0.5}O_4$ samples after the first firing step at various temperatures. Even at a preparation temperature of 350° C, there is evidence of spinel formation, although Mn_2O_3 is still prevalent as an impurity phase at this temperature. At higher temperatures, the impurity levels of Mn_2O_3 decrease; the spinel peaks sharpen and increase in intensity, indicative of an increase in crystallinity. Note that Li_2MnO_3 appears only in the 750 °C sample in very minor concentration.

The $LiMn_{1.5}Cu_{0.5}O_4$ samples prepared at 350 °C and 500 °C were each subsequently refired at 650° and 750 °C. The X-ray diffraction patterns of these materials are shown in Figures 3 and 4, respectively. Refiring at 650 °C resulted in the incorporation of most of the unreacted manganese oxides into the spinel structure; a final 750 °C soak was necessary to complete the reaction. This firing sequence produced what appeared to be essentially phase-pure materials (Figures 1 and 4); the X-ray data show a small, but significant [220] peak at 39° 2θ. The intensity of this peak indicates that a small amount of copper resides on the 8a tetrahedral sites of the spinel structure.

The neutron diffraction pattern of a $LiMn_{1.5}Cu_{0.5}O_4$ sample is shown in Figure 5. The data show clear evidence of a spinel phase (solid line) and an impurity phase (dotted line). The peaks of the impurity phase are also highlighted by an expanded region of the data (inset in Figure 5) and the difference profile, shown below the neutron diffraction pattern, which was obtained by subtracting the spinel peaks from the pattern. The composition of the spinel component in the sample as determined by X-ray diffraction analysis (described in a following section) indicated that the impurity phase was a lithium-copper-oxide compound. The appearance of the impurity only in the neutron diffraction pattern was attributed to the fact that copper is a very strong scatterer of neutrons ($b=0.78 \times 10^{12}$ Å). The observation of the impurity phase only in the neutron diffraction pattern highlights the possible dangers of misinterpreting X-ray diffraction patterns.

Electrochemical studies

The potential limits that were used for the electrochemical cycling of $Li/LiMn_{2-x}Cu_xO_4$ cells were 3.3 - 5.1 V. In general, the charge capacity of the spinel electrode exceeded the

discharge capacity by 5 - 10% on the first 10 cycles; this coulombic inefficiency was attributed to slight electrolyte oxidation at the higher potentials. Figure 6 shows the voltage profiles obtained for the various Li/$LiMn_{2-x}Cu_xO_4$ cells ($0 \leq x \leq 0.5$) during the third cycle. The total capacity of $LiMn_{2-x}Cu_xO_4$ electrodes drops with increasing copper content from 119 mAh/g at $x = 0.1$ to 71 mAh/g at $x = 0.5$.

Table 1 summarizes the relative amounts of capacity obtained in the high voltage region (5.1-4.5 V) and low voltage region (4.5-3.3 V) during the third discharge. Figure 7 shows the cyclic voltammograms of the spinel series. Note that the spinel composition with the lowest copper content ($LiMn_{1.9}Cu_{0.1}O_4$) provides a voltage profile and cyclic voltammogram which closely resembles those obtained from standard $LiMn_2O_4$ (14). As the copper content of the spinel increases, the peaks which are located at 4.05 and 4.16 V in the cyclic voltammogram of $LiMn_2O_4$, (attributed to a two-step extraction of lithium from the tetrahedral 8a sites), shift to higher voltages. The higher voltage peak splits into a doublet. These features are particularly noticeable in the $LiMn_{1.5}Cu_{0.5}O_4$ sample in which the higher voltage peak (at 4.16 V in $LiMn_2O_4$) is shifted and split into two peaks at approximately 4.22 and 4.30 V. Although the reasons for this behavior are not yet fully understood, it is believed that the peak shifts are associated with the presence of some copper on the tetrahedral sites of the spinel structure. It is possible that one of the higher voltage peaks of the doublet may be due to oxidation of the lithium-copper-oxide impurity phase. The high voltage reaction at 4.9 V that increases with increasing copper content is attributed to the oxidation of Cu^{2+} to Cu^{3+} on the octahedral (16d) sites of the spinel structure. The cyclic voltammograms indicate that all these reactions appear to be reversible, at least on the first cycle.

It is clear that copper substitution has two major effects on the electrochemistry of the spinel electrode that can be interpreted in terms of the coordination and oxidation state of the copper ions. If mimicked Amine's nickel-substituted analog, $Li[Mn_{1.5}Ni_{0.5}]O_4$, (16), the copper ions would all be divalent and the manganese ions would be fully-oxidized in a tetravalent state. In this circumstance, no charge capacity would be expected in the 3.9 - 4.3 V region, which originates from $Mn^{3+} \rightarrow Mn^{4+}$ oxidation; if the 4.9 V plateau was attributed to $Cu^{2+} \rightarrow Cu^{3+}$ oxidation, then a maximum capacity of 70 mAh/g would be expected at this voltage. The electrochemical data shown in Figures 6 and 7 is clearly inconsistent with a spinel electrode with the simple cation arrangement in $Li[Mn_{1.5}Cu_{0.5}]O_4$; the data imply a different cation arrangement and charge distribution in the structure of the spinel electrode. The relatively large capacity that is obtained between 3.9 and 4.4 V for $LiMn_{2-x}Cu_xO_4$ compounds with small x is associated with a large Mn^{3+} concentration on the octahedral sites (Table 1). The relatively low capacity that is obtained at 4.9 V but which increases with increasing x, and the fact that the overall achievable capacity declines sharply with increasing x is consistent with increasing Cu^{2+} and Mn^{4+} concentrations in the spinel samples.

Figure 8 shows the cycling performance in terms of discharge/charge capacity obtained between 5.1 and 3.3 V, expressed in mAh/g, *vs.* cycle number for the series of $LiMn_{2-x}Cu_xO_4$ electrodes ($0 \leq x \leq 0.5$). The available capacity decreases as the amount of copper in the spinel increases. However, electrodes with higher copper content showed significantly improved capacity retention on cycling. For example, Li/"$LiMn_{1.9}Cu_{0.1}O_4$" cells show on average, an initial capacity of 120 mAh/g which decreases to 103 mAh/g after 70 cycles, reflecting a 14% loss,

whereas Li/"$LiCu_{0.5}Mn_{1.5}O_4$" cells show an initial capacity of 71 mAh/g that fades to 65 mAh/g over the same number of cycles (8% loss).

XANES measurements

Figure 9 shows the XANES spectra at the Mn K edge for Mn, MnO, Mn_2O_3, MnO_2 and $LiMn_{1.5}Cu_{0.5}O_4$. The MnO_2 spectra were obtained from a chemically-prepared MnO_2 sample (CMD). Data for electrochemically-prepared MnO_2 (EMD) are almost identical. The XANES data for $LiMn_{1.5}Cu_{0.5}O_4$ (dotted line), which show a shoulder on the main peak at 11.5 eV, are consistent with the presence of both Mn^{4+} and Mn^{3+}, implying that Mn^{3+} exists in a relatively low concentration in the spinel structure. Figure 10 shows the XANES spectra at the Cu K-edge for Cu foil, Cu_2O, CuO and $LiCu_{0.5}Mn_{1.5}O_4$. The spectrum for CuO has a distinct shoulder at 8 eV. This is due to the distorted octahedral coordination of Cu. Each Cu is surrounded by four planar O atoms at a distance of 1.96 Å and two axial O atoms at a distance of 2.78 Å. The shoulder at 8 eV has been attributed to transitions from the 1*s* state to the axial 4*p* states, and the peak at 18 eV to transitions to the planar 4*p* states (23). In a more symmetrical coordination such as an aqueous solution of Cu^{2+} the shoulder at 8 eV disappears, but the position of the white line peak at 18 eV remains unchanged (23). Theoretical calculations predict that for Cu^{3+} the white line should shift by 10 eV in going from Cu^{2+} to Cu^{3+} (24). Measurements on $KCuO_2$, in which the Cu^{3+} ions have square planar coordination to neighboring, show a peak shift of only 4 eV (23). Since no shift is seen in the peak, and there is no shoulder in the edge, the XANES data would appear to indicate only Cu^{2+} ions with a symmetric coordination.

Structure Refinements

The lattice parameter, *a*, of $LiMn_{2-x}Cu_xO_4$ spinel structures, decreases with increasing x, from 8.234Å in $LiMn_2O_4$ (x=0), through 8.212Å in "$LiMn_{1.7}Cu_{0.3}O_4$" (x=0.3) to 8.199 Å in "$LiMn_{1.5}Cu_{0.5}O_4$" (x=0.5) (Figure 11); this trend is characteristic of an increasing concentration of Mn^{4+} ions in the spinel structure which results from the substitution of Mn^{3+} ions by Cu^{2+} ions.

In a spinel structure with the cation distribution $Li[Mn_{1.5}Cu_{0.5}]O_4$, charge neutrality is obtained when the manganese ions are all tetravalent and the copper ions are all divalent. Replacement of copper by lithium on the octahedral sites results in $Li_4Mn_5O_{12}$ (or in spinel notation $Li[Mn_{1.67}Li_{0.33}]O_4$) in which charge neutrality is achieved by increasing the Mn^{4+} content to compensate for the monovalent lithium ions. These two compounds are, in principle the end-members of a possible solid solution system $Li[Mn_{1.5+x}Cu_{0.5-3x}Li_{2x}]O_4$ ($0 \leq x \leq 0.167$). In this solid solution system, it would also be possible for lithium and copper ions to exchange on the tetrahedral sites. Structural refinements of such complex systems are difficult, particularly when three different cation-types are disordered over one crystallographically independent site. Despite the difficulties that were encountered in obtaining a meaningful fit to the neutron diffraction data of a two-phase reaction product, these analyses provided valuable information about the structure that could not be determined from the X-ray diffraction patterns. This information was then used for the final structure refinement with the "single-phase" X-ray diffraction data. The structure was refined using the prototypic cubic spinel space group Fd3m.

Structure analyses of the spinel component in two independent $LiMn_{1.5}Cu_{0.5}O_4$ samples using neutron diffraction data from Argonne National Laboratory and the Rutherford Laboratory showed unequivocally, and consistently with various models, that some copper occupied the 8a tetrahedra with a site occupancy of approximately 0.1. Furthermore, refinements of various models showed consistently that between 1.64 and 1.71 Mn occupied the octahedral B sites of the $A[B_2]O_4$ spinel structure. A site occupancy of 0.835, corresponding to an average 1.67 Mn in the $[B_2]O_4$ spinel framework was, therefore, used for the refinement of the X-ray data. It is, perhaps, significant that this value corresponds to the Mn content in $Li_4Mn_5O_{12}$ ($Li[Mn_{1.67}Li_{0.33}]O_4$).

The initial refinements of the X-ray data showed that the intensity of the [220] peak at approximately 31° 2θ could not be accounted for by placing only lithium on the tetrahedral sites, consistent with the neutron data. Subsequent refinements were, therefore, carried out on the system $(Li_{0.9}Cu_{0.1})_{8a}[Mn_{1.67}Cu_{0.33-\delta}Li_{\delta}]_{16d}O_{4-\alpha}$ using the input from the neutron data. The parameter, δ, was used to control the stoichiometry of the lithium and copper on the 16d octahedral sites. A second parameter, α, was refined to determine if there was any non-stoichiometry in the oxygen content. Because of the limited number of the reflections (intensity data), isotropic temperature factors (U) were assigned to all the ions. The cations were constrained to have the same U value.

The results of the refinement which yielded the best fit to the data (R_p=8.7%) are summarized in Table 2. The observed and calculated powder X-ray diffraction profiles of the spinel component in the $LiMn_{1.5}Cu_{0.5}O_4$ sample for this refinement are shown in Figure 12. The

lattice parameter refined to 8.1923(2) Å. Refinements of two separate samples did not favor an oxygen-deficient structure; both refinements showed that the oxygen ion positions were fully occupied (α=0). The structure analysis showed a cation distribution $(Li_{0.9}Cu_{0.1})_{8a}[Mn_{1.67}Cu_{0.22}Li_{0.11}]_{16d}O_4$; the overall composition is $Li_{1.01}Mn_{1.67}Cu_{0.32}O_4$. Assuming that all the copper is divalent, then the oxidation state of the manganese ions is 3.80; this finding is consistent with the XANES data that indicated only a small Mn^{3+} ion concentration in the "$LiMn_{1.5}Cu_{0.5}O_4$" samples.

A spinel electrode with the composition $(Li_{0.9}Cu_{0.1})_{8a}[Mn_{1.67}Cu_{0.22}Li_{0.11}]_{16d}O_4$ would have a theoretical capacity of 95 mAh/g, corresponding to the extraction of 0.65 Li^+ ions and the complete oxidation of 0.33 mole fraction Mn^{3+} to Mn^{4+} and 0.22 mole fraction Cu^{2+} to Cu^{3+}. The capacity associated with the manganese and copper ions on the octahedral sites is 48 and 32 mAh/g, respectively, which is in good agreement with the capacities of 48 and 23 mAh/g obtained from this electrode in an electrochemical cell (Table 1). The experimentally achieved capacity reflects, therefore, a 75% utilization of the theoretical capacity. The possibility of exceeding this capacity appears to be limited because it is anticipated that the oxidation of Cu^{2+} ions on tetrahedral sites would occur at a voltage >5 V which is above the stability window of the electrolyte.

If all the manganese present in the precursor materials was used in the fabrication of the spinel structure, as implied by the repeated firings required to completely react the manganese oxides (Figures 3 and 4), then the composition $Li_{1.01}Mn_{1.67}Cu_{0.32}O_4$ indicates that 9% of the lithium and 42% of the copper in the precursor materials were not incorporated into the spinel framework.

This result strongly suggests that the impurity detected in the neutron diffraction profile is a lithium copper oxide phase. Although several lithium copper oxide compounds are known to exist, particularly $Li_2O{\bullet}nCuO$ compounds with divalent copper, such as $Li_2Cu_2O_3$ (n=2) (25) and Li_2CuO_2 (n=1) (26), none of these compounds could be indexed satisfactorily to all the peaks of the impurity phase in the neutron diffraction pattern.

Morphological characterization of $LiMn_{2-x}Cu_xO_4$ spinels

Scanning electron micrographs of spinel samples in the $LiMn_{2-x}Cu_xO_4$ series ($0 \leq x \leq 0.5$), prepared by solid state reactions, are presented in Figure 13(a-d). The products, which include the standard, unmodified $LiMn_2O_4$ spinel (x=0) (Figure 13a) all possess an onion-like microstructure with an approximate 2 μm ring thickness. These onion-like structures can be expected to be subject to cracking and exfoliation during electrochemical cycling, unless the "breathing" that is expected to occur during lithium intercalation and deintercalation can be minimized. At this stage, the extent of morphological changes (and variations in lattice parameter and crystal symmetry) of the copper-substituted spinels that occur during lithium extraction and insertion reactions is unknown. Further work is being planned to monitor the changes in crystal morphology of these structures to long-term electrochemical cycling.

Thermo-gravimetric analysis of $LiMn_{1.5}Cu_{0.5}O_4$ under hydrogen

Thermogravimetric analysis measurements were conducted to investigate the thermal stability of $LiMn_{1.5}Cu_{0.5}O_4$ relative to $LiMn_2O_4$ under reducing conditions (H_2) (Figure 14); the data show significant differences, both in the onset temperature and the degree of reduction. The

reduction of $LiMn_2O_4$ that occurs through oxygen loss is initiated at approximately 140 °C; over the next 200 °C, the sample loses 9.6% of its weight. Following a lengthy period of minimal weight loss, the material undergoes a further weight loss of 4.6% from 820 ° to 900 °C. The first reduction process corresponds to the removal of approximately one oxygen atom from the spinel formula unit, resulting in "$LiMn_2O_3$" (the theoretical weight loss for this reaction is 8.9%). The total weight loss of 14.2% corresponds closely to the formation of "$LiMn_2O_{2.5}$", alternatively "$Li_2O{\cdot}4MnO$" (the theoretical weight loss for this reaction is 13.3%).

Inclusion of copper in the spinel framework dramatically increases the reactivity towards hydrogen. Onset of weight loss was almost immediate, and by 230°C, the $LiMn_{1.5}Cu_{0.5}O_4$ sample had lost 26% of its weight, indicating that the residue had the empirical formula $LiMn_{1.5}Cu_{0.5}O_{1.0}$. Subsequent heating to 900 °C resulted in an additional 3.5% weight loss, mostly above 750 °C. The result indicates that the reduced product of $LiMn_{1.5}Cu_{0.5}O_4$ at 900 °C is comprised essentially of metallic Cu and Mn, and Li_2O (the theoretical weight loss for the reaction is 30.2%); moreover, the result demonstrates that the presence of copper in the spinel greatly facilitates electron transfer within the spinel framework which, at moderate temperatures (200 ° -300 °C), leads to an almost complete reduction of $LiMn_{1.5}Cu_{0.5}O_4$.

Conclusions

Novel electroactive materials, $LiMn_{2-x}Cu_xO_4$, ($0.1 \leq x \leq 0.5$) have been prepared and evaluated in lithium cells. The data show that lithium can be extracted from the spinel structures in two main potential regions: 3.9 to 4.3 V and 4.8 to 5.0 V, attributed to the oxidation

of Mn^{3-} to Mn^{4+} and Cu^{2+} to Cu^{3+}, respectively. The reactions are reversible. Stable electrochemical cycling has been observed for electrode compositions with high values of x, but with low capacity (60-70 mAh/g), for example, in an electrode with overall composition "$LiMn_{1.5}Cu_{0.5}O_4$" (x=0.5). Analysis of X-ray and neutron diffraction data, and XANES spectra have revealed that it is difficult to synthesize single-phase lithium-copper-manganese-oxide spinel compounds with a predetermined composition. The stability and relatively low reactivity of CuO (compared to Li_2O) appears to restrict the complete incorporation of copper into the spinel structure. The cation distribution in these spinel structures is highly complex, which makes it difficult to perform detailed structure analyses with X-ray and neutron diffraction data with a high degree of accuracy. Although the XANES data show that the oxidation state of copper in these spinel compounds is divalent, the possibility of a small amount of Cu^{1+} (in tetrahedral sites) or Cu^{3+} (in octahedral sites) in the starting spinel structures should not be entirely discounted. *In-situ* XANES and X-ray diffraction experiments are being planned in order to obtain further information about the structural properties of these spinel compounds.

Acknowledgments

This work was performed under an SBIR Phase I DoD program sponsored by the U.S. Army CECOM, administered by the Army Research Laboratory, Fort Monmouth, NJ, under Contract No. DAABO7-97-C-D304. Support for Argonne National Laboratory from the U.S. Department of Energy's Advanced Battery Program, Chemical Sciences Division, Office of Basic Energy Sciences, under Contract No. W-31-109-Eng-38 is gratefully acknowledged. Dr. W. I. F. David and Dr. R. M. Ibberson are thanked for collecting neutron diffraction data at the

Rutherford Appleton Laboratory and for undertaking some preliminary structural refinements. The authors would like to thank Mrs. J. H. Hemenway and Mr. R. Laura for assisting in manuscript preparation and Professor. J. B. Goodenough for stimulating discussions.

References

1. J. R. Dahn, T. Zheng, Y. Liu, and J. S. Xue, *Science*, **270**, 590 (1995).
2. R. Yazami, presented at 12th Int. .Seminar, Primary and Secondary Battery Technology and Applications, Deerfield Beach, FL, 6-9 March 1995.
3. Y. Idota, T. Kubota, A. Matsufuji, Y. Maekawa and T. Miyasaki, *Science,* **276**, 1395 (1997).
4. J. B. Goodenough, D. G. Wickham, and W. J. Croft, *J. Phys. Chem. Solids,* **5**, 107 (1958).
5. K. Mizushima, P. C. Jones, P. J. Wiseman, and J. B. Goodenough, *Mat. Res. Bull.*, **15**, 783 (1980).
6. E. Plitcha, M. Salomon, S. Slane, M. Uchiyama, D. Chua, W. B. Ebner, and H. W. Lin, *J. Power Sources*, **21**, 25 (1987).
7. J. R. Dahn, U. von Sacken, and C. A. Michal, *Solid State Ionics*, **44**, 87 (1990).
8. A. Lecerf, M. Broussely, and J. P. Gabano, *U.S. Patent No. 4 980 080*, 1989.
9. T. Nagaura, *JEC Battery Newsletter*, No. 2 (Mar. - Apr.) (1991).
10. ITE Battery Newsletter, No. 6 (Nov. - Dec.) (1996).
11. M. M. Thackeray, Progress in Batteries and Battery Materials, Vol. 14, R. J. Brodd, ed., ITE Press, Inc., Brunswick, OH, p.1 (1995), and references therein.
12. R. J. Gummow, A. de Kock, D. C. Liles, and M. M. Thackeray, *Solid State Ionics*, **69**, 59 (1994).
13. G. Pistoia, C. Bellito, and A. Antonini, 190th Electrochem. Soc. Meeting, San Antonio, TX, 6-11 October 1996.
14. A. D. Robertson, S. H. Lu, and W. F. Howard, Jr., *J. Electrochem. Soc.*, in press.
15. I. J. Davidson, R. S. McMillan, and J. J. Murray, *U.S. Patent No. 5 370 949*, 1994.

16.K. Amine, H. Tukamoto, H. Yasuda, and Y. Fujita, 188th Electrochem. Soc. Meeting, Chicago, IL 8-13 October 1995; K. Amine, H. Tukamoto, H. Yasuda, and Y. Fujita, *J. Electrochem. Soc.*, **143**, 1607 (1996).

17.C. Sigala, D. Guyomard, A. Verbaere, Y. Piffard and M. Tournoux, Solid State Ionics, **81**, 167 (1995).

18.Y. Gao, K. Myrtle, M. Zhang, J. N. Reimers, and J. R. Dahn, *Phys. Rev. B*, **54**, 3878 (1996).

19.Y. Ein-Eli and W.F. Howard, Jr., *J. Electrochem. Soc.*, **144**, L205 (1997).

20.K.I. Pandya, R.W. Hoffman, J. McBreen, and W.E. O'Gradey, *J. Electrochem. Soc.*, **137**, 383 (1990).

21.J. Wong, F.W. Lytle, R.P. Mssmer, and D.H. Maylotte, *Phys. Rev.*, **B 30**, 5596 (1984).

22.A.C. Larson and R.B. Von Dreele "GSAS-General Structure Analysis System". Rept. LA-UR-86-748, Los Alamos National Laboratory, Los Alamos, nm 87548, 1990.

23.J.M. Tranquada, S.M. Heald, and A.R. Moodenbaugh, *Phys.Rev.*, **B 36**, 5263 (1987).

24.E.E. Alp, G.K. Shenoy, D.G. Hinks, D.W. Capone II, L. Soderholm, H.B. Schuttler, J. Guo, D.E. Ellis, P.A. Montano, and M. Ramanathan, *Phys. Rev.* **B 35**, 7199 (1987).

25.JCPDS Data File 36-661.

26.J. Barker and M. Yazid Saidi, U.S. Patent 5,670,277 (1997).

Figure Captions

Figure 1: XRD patterns obtained from $LiCu_{0.5}Mn_{1.5}O_4$ spinel prepared by solid state and sol-gel preparation methods. The XRD pattern of unmodified $LiMn_2O_4$ spinel is shown for comparison.

Figure 2: XRD patterns obtained from $LiCu_{0.5}Mn_{1.5}O_4$ prepared *via* sol gel method at one calcining temperature, as listed.

Figure 3: XRD patterns of $LiCu_{0.5}Mn_{1.5}O_4$ prepared *via* sol-gel method with calcining temperature of 350°C which was subsequently refired at 650 and 750°C.

Figure 4: The same as Figure 3. Calcining temperature of 500°C.

Figure 5: Refined neutron diffraction pattern for $Li_{1.01}[Mn_{1.67}Cu_{0.32}]O4$. The data is shown as small dots, the calculated pattern (based on the reported model) is shown as a solid line, and the difference between the calculated and observed data is shown below the diffraction pattern. The inset in the upper right hand corner show in more detail the region from 7.3 msec and the impurity phase in the material can be clearly seen in the difference profile. The tick marks in the spectra identify the peaks from the spinel phase.

Figure 6: The potential (V) - capacity (mAh/g) curves obtained from the third cycle for $LiCu_xMn_{2-x}O_4$ ($0 \leq x \leq 0.5$) in steps of $x = 0.1$. Li metal served as counter electrode in EC(2):DMC(3)/1.2M $LiPF_6$.

Figure 7: Cyclic voltammogram obtained from $LiCu_xMn_{2-x}O_4$ ($x = 0$, 0.1, 0.3, 0.4 and 0.5) cycled in the potential limits of 3.75 - 5.2 V at scan rate of 15 μV/s. Li metal served both as counter and reference electrode in EC(2):DMC(3)/1.2M $LiPF_6$.

Figure 8: The cycle life behavior (charge/discharge capacity, expressed in mAh/g *vs.* cycle number) of $LiCu_xMn_{2-x}O_4$ ($0 \leq x \leq 0.5$, in steps of $x = 0.1$). Li metal served as a counter electrode in EC(2):DMC(3)/1.2 M $LiPF_6$.

Figure 9: Normalized Mn K edge XANES for Mn (—————), MnO (·····), Mn_2O_3 (- - -), MnO_2 (---), and $LiCu_{0.5}Mn_{1.5}O_4$ (····).

Figure 10: Normalized Cu K edge XANES for Cu foil (————), Cu_2O (- - -), CuO (·····), and $LiCu_{0.5}Mn_{1.5}O_4$ (····).

Figure 11: Cubic cell dimension for $LiCu_xMn_{2-x}O_4$ ($0 \leq x \leq 0.55$) as a function of x.

Figure 12: .Powder X-ray diffraction pattern of $LiMn_{1.5}Cu_{0.5}O_4$ using CuK. The structure was refined using the protoypic cubic spinel space group Fd3m The observed data points are depicted as small dots, and the line through them is the calculated pattern based on the refined model. The difference between the observed and calculated patterns is shown below the profiles.

Figure 13: SEM micrographs obtained from (a) $LiMn_2O_4$; (b) $LiCu_{0.2}Mn_{1.8}O_4$; (c) $LiCu_{0.4}Mn_{1.6}O_4$; and (d) $LiCu_{0.5}Mn_{1.5}O_4$.

Figure 14: TGA profiles (30 to 900°C at 5°C/min. in H_2) of $LiMn_2O_4$ and $LiCu_{0.5}Mn_{1.5}O_4$.

Table I: Relative Capacities of Empirical "$LiCu_xMn_{2-x}O_4$" Electrodes

x in $LiCu_xMn_{2-x}O_4$	Capacity, mAh/g at 5.1-4.5V	Capacity, mAh/g at 4.5-3.3V	Cu:Mn Capacity Ratio
0.1	7	112	1:16
0.2	10	96	1:10
0.3	13	79	1:6
0.4	19	63	1:3
0.5	23	48	1:2

Table II: Crystallographic parameters of $(Li_{0.9}Cu_{0.1})_{8a}[Mn_{1.67}Cu_{0.33-\delta}Li_{\delta}]_{16d}O_4$ (Space group Fd3m, a = 8.1923(2) Å; Vol.= 549.82(2) Å^3) [Rp=8.7%]

Atom	Wyckoff Notation	x	y	z	U (x100)	Site Occupancy, n
Li (1)	8a	0.125	0.125	0.125	2.42(6)	0.9
Cu (1)	8a	0.125	0.125	0.125	2.42(6)	0.1
Mn (1)	16d	0.5	0.5	0.5	2.42(6)	0.835
Cu (2)	16d	0.5	0.5	0.5	2.42(6)	0.112(6)
Li (2)	16d	0.5	0.5	0.5	2.42(6)	0.053(6)
O (2)	32e	0.2652(2)	0.2652(2)	0.2652(2)	3.63(7)	1

Figure 1

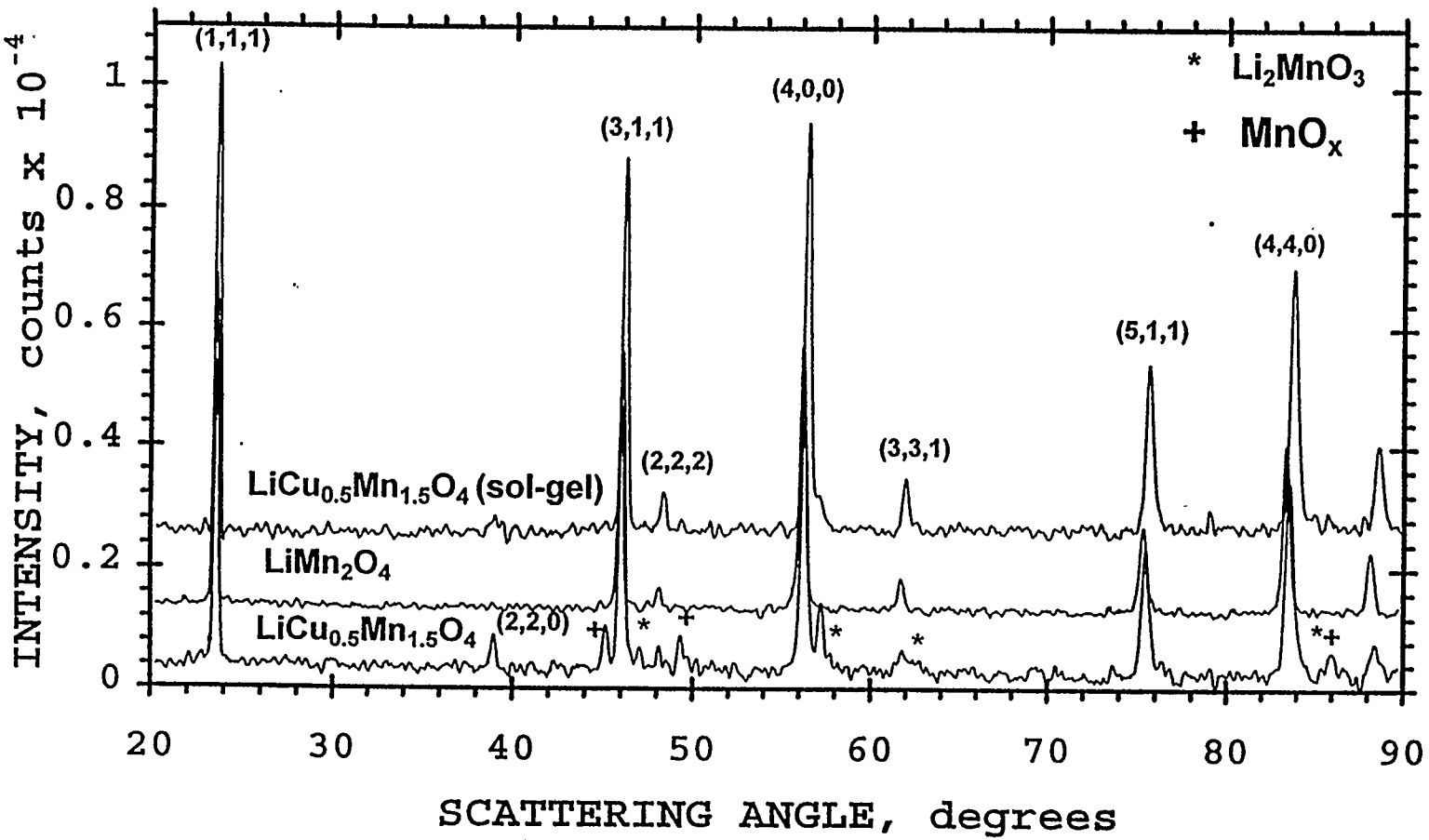

Figure 1

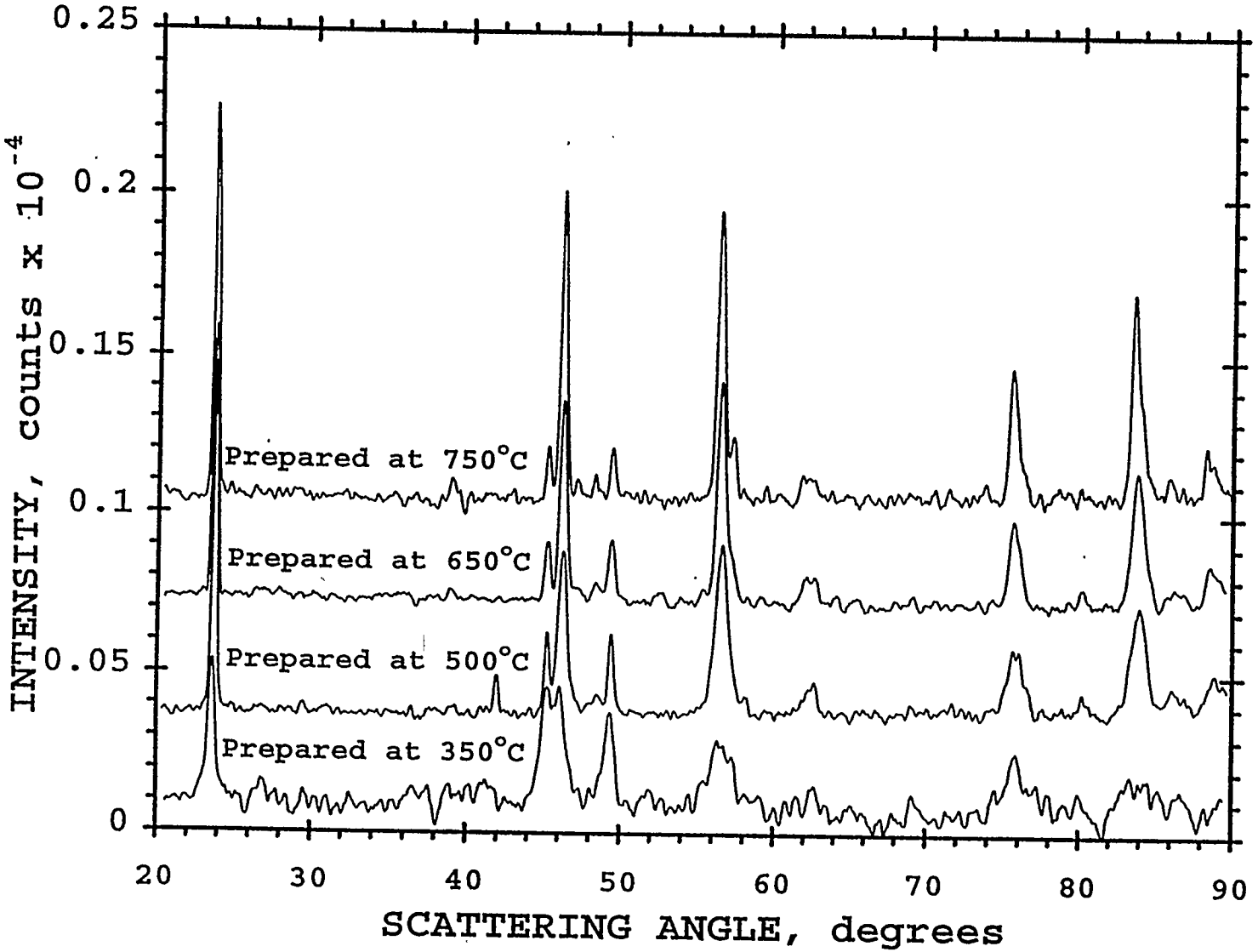
0.25
0.2
0.15
0.1
0.05
0
INTENSITY, counts x 10^{-4}
Prepared at 750°C
Prepared at 650°C
Prepared at 500°C
Prepared at 350°C
20
30
40
50
60
70
80
90
SCATTERING ANGLE, degrees

Figure 2

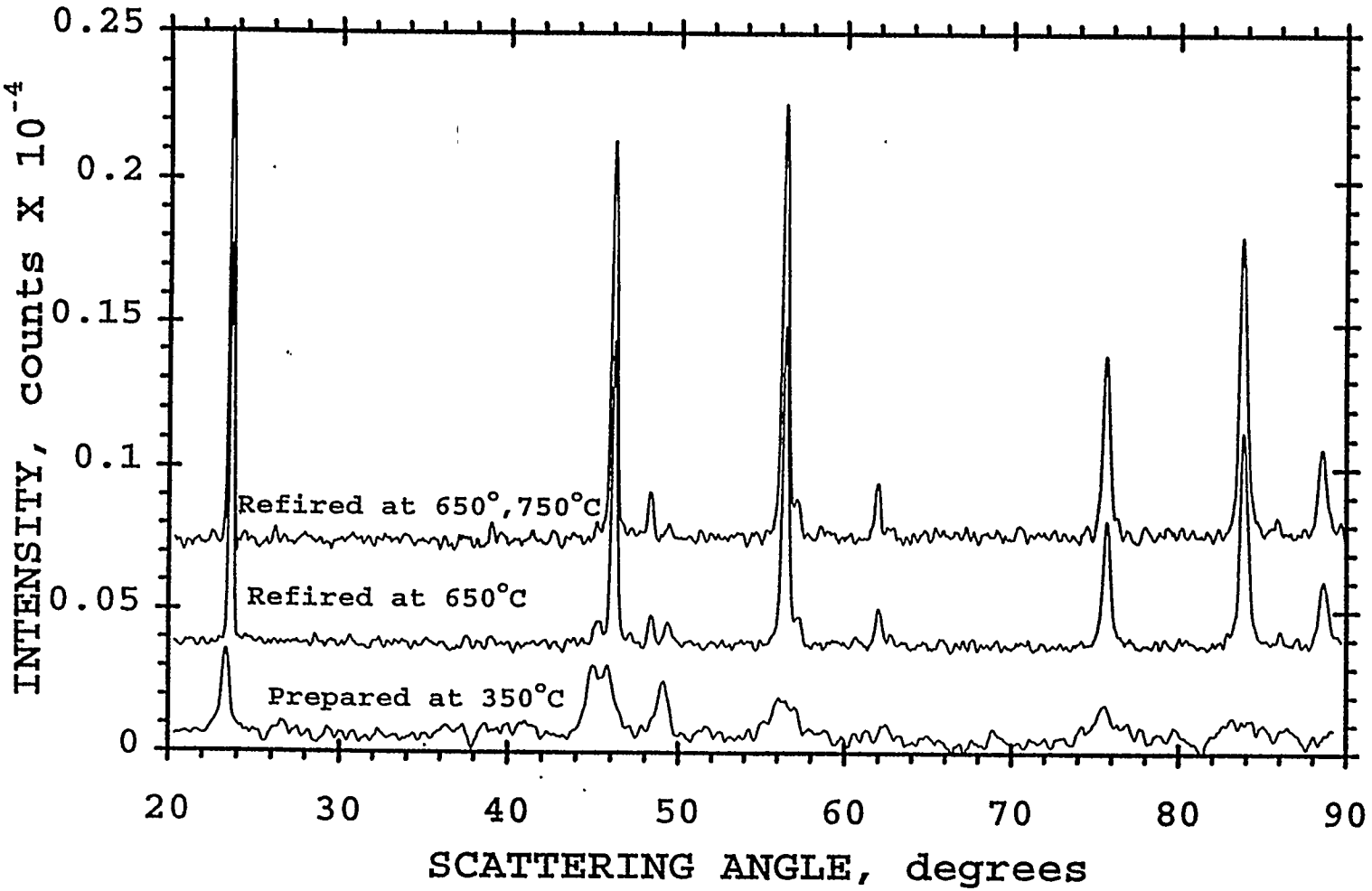
0.25
0.2
0.15
0.1
0.05
0
INTENSITY, counts X 10^-4
Refired at 650°,750°C
Refired at 650°C
Prepared at 350°C
20
30
40
50
60
70
80
90
SCATTERING ANGLE, degrees

Figure 3

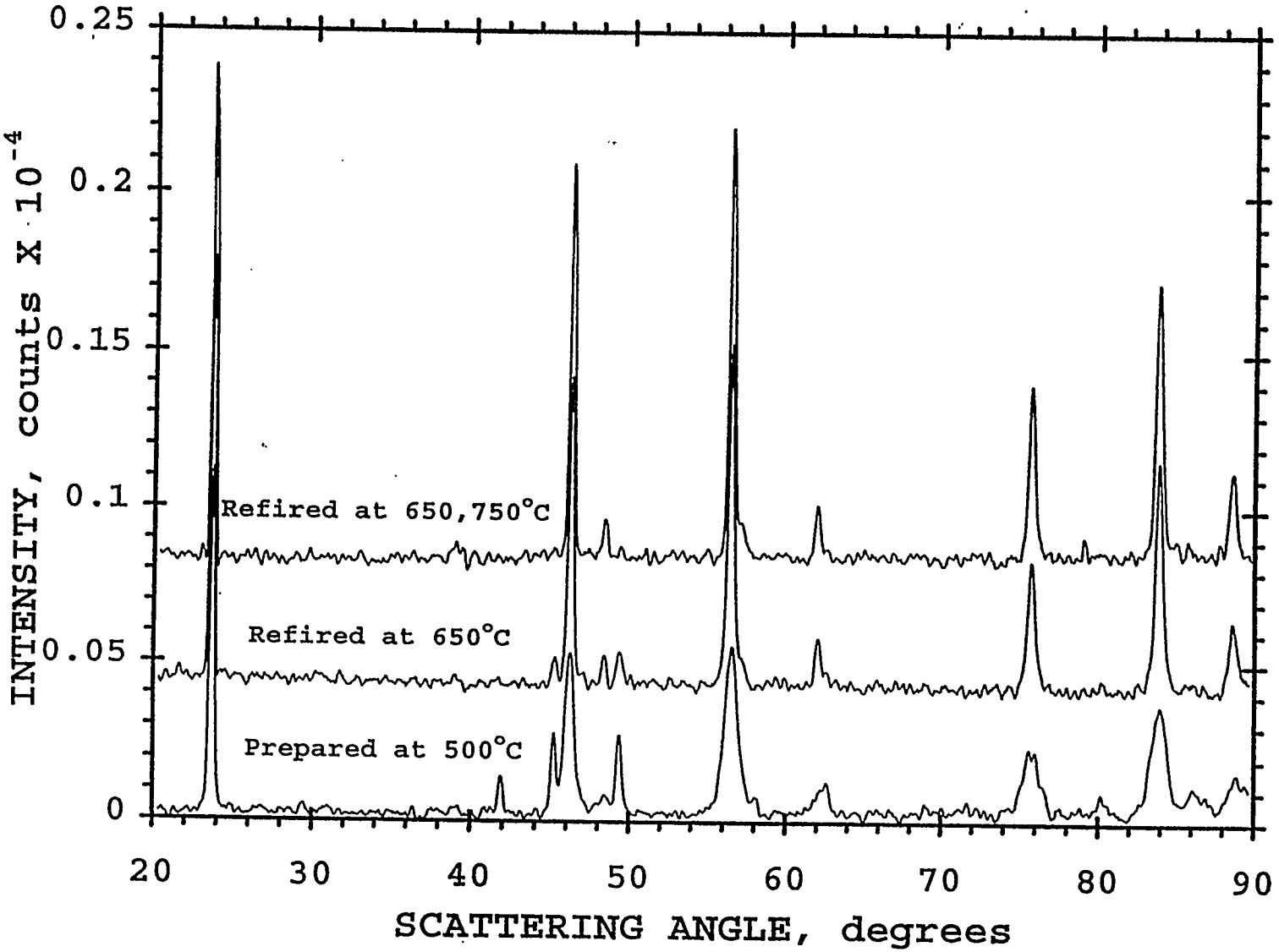
0.25
0.2
0.15
0.1
0.05
0
INTENSITY, counts X 10^{-4}
Refired at 650,750°C
Refired at 650°C
Prepared at 500°C
20
30
40
50
60
70
80
90
SCATTERING ANGLE, degrees

Figure 4

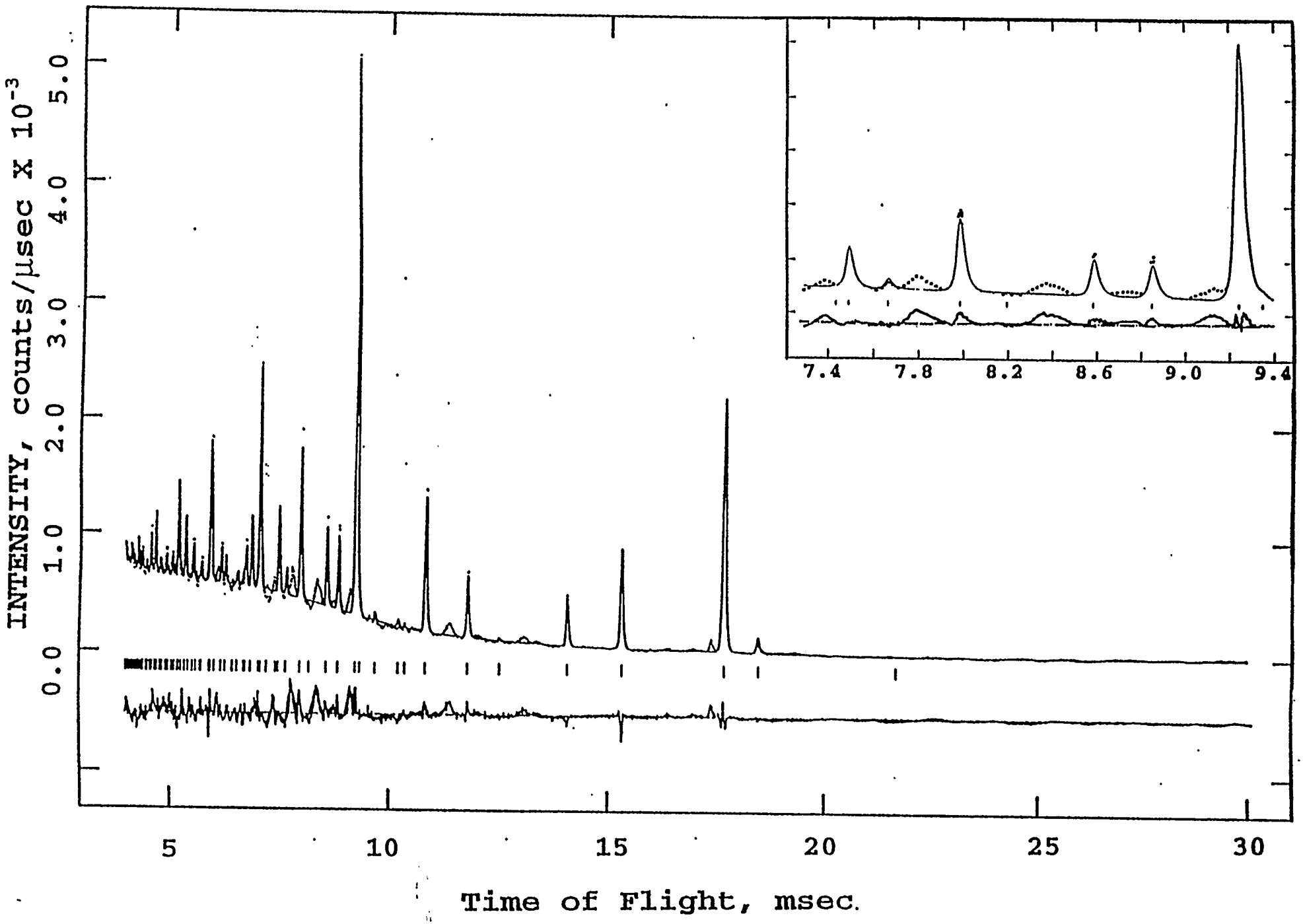
INTENSITY, counts/μsec X 10^{-3}
0.0
1.0
2.0
3.0
4.0
5.0
5
10
15
20
25
30
Time of Flight, msec.
7.4
7.8
8.2
8.6
9.0
9.4

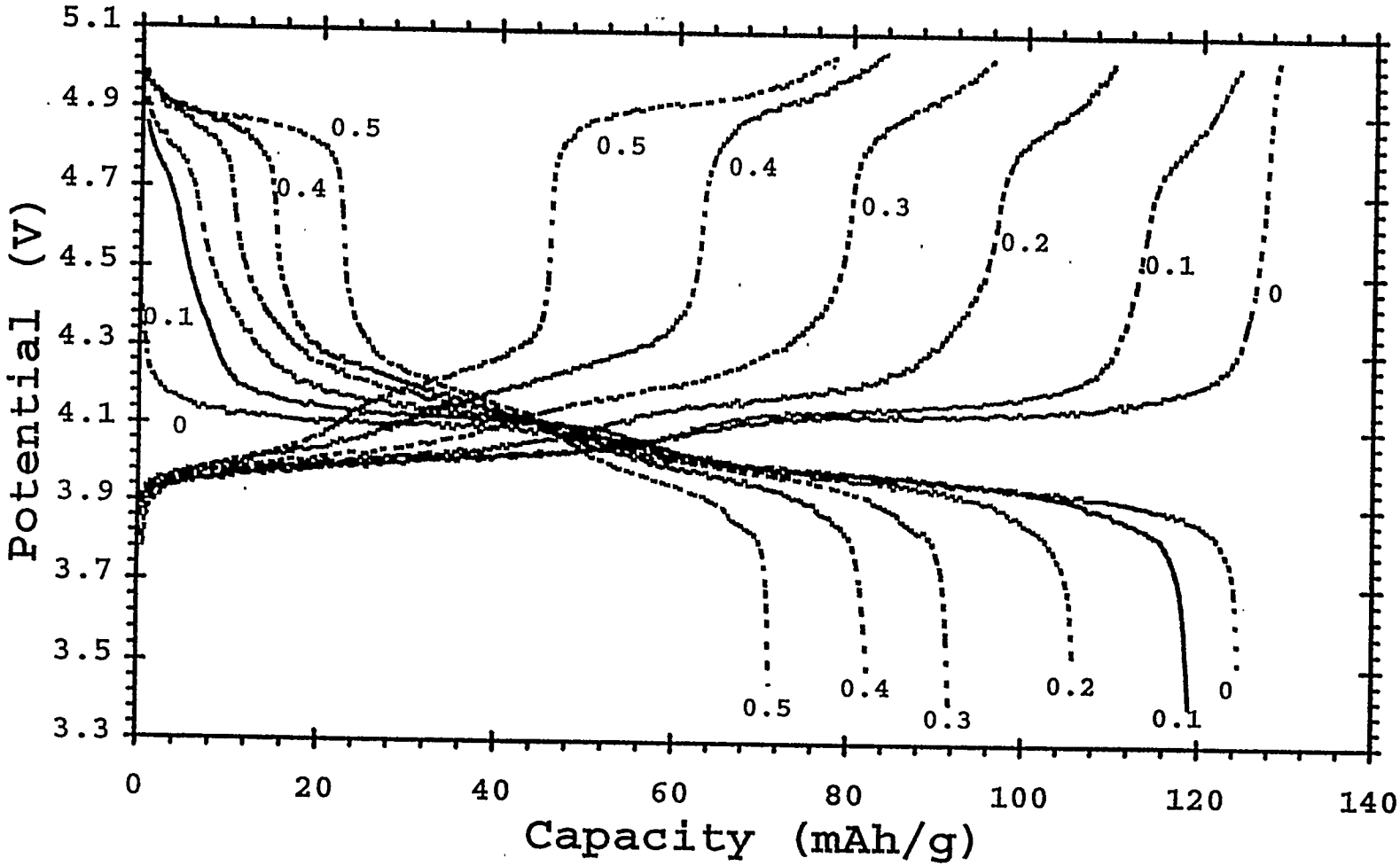
Potential (V)
5.1
4.9
4.7
4.5
4.3
4.1
3.9
3.7
3.5
3.3
0
20
40
60
80
100
120
140
Capacity (mAh/g)
0.5
0.4
0.1
0
0.5
0.4
0.3
0.2
0.1
0
0.5
0.4
0.3
0.2
0.1
0

Figure 6

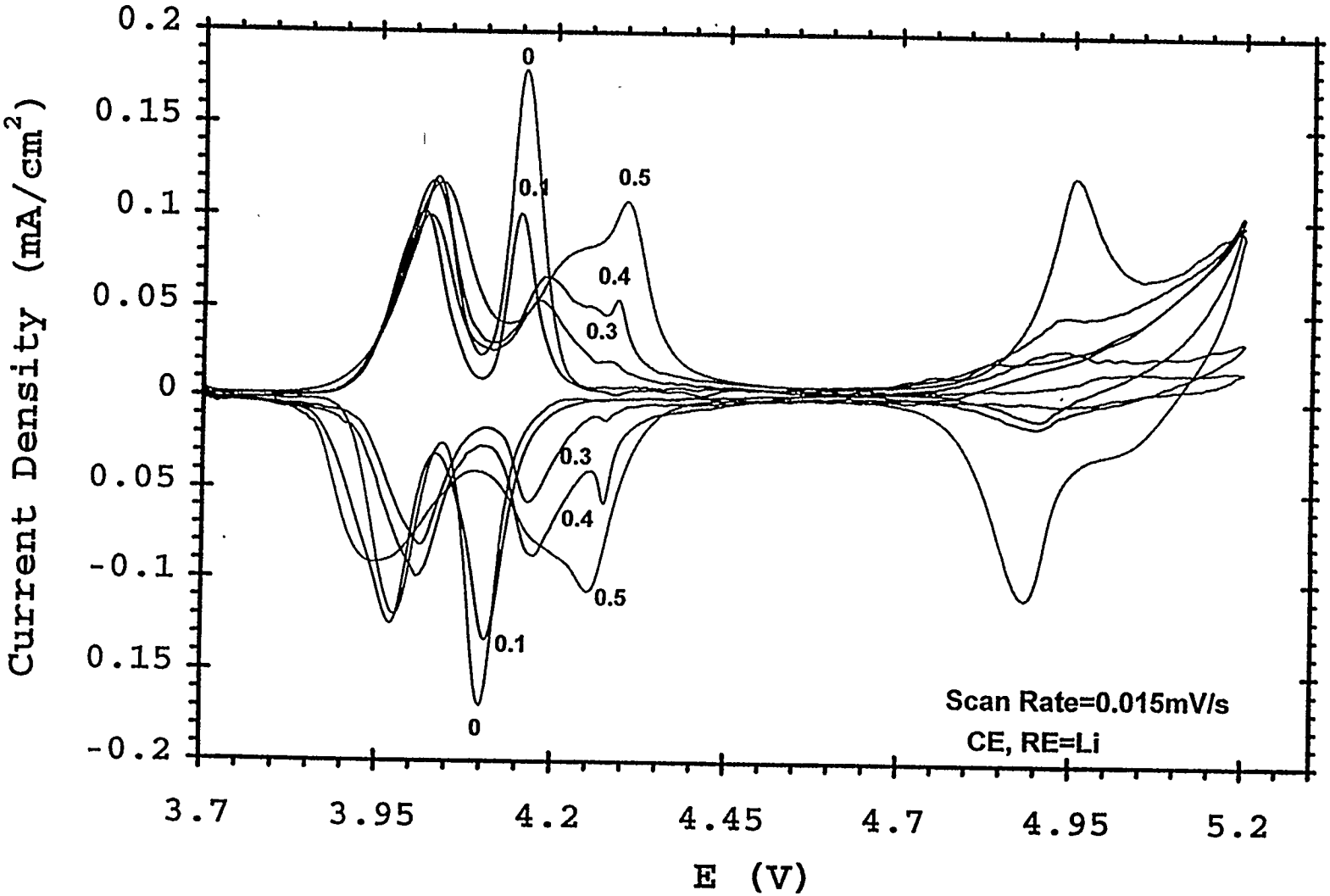
Current Density (mA/cm^2)
0.2
0.15
0.1
0.05
0
0.05
-0.1
0.15
-0.2
3.7
3.95
4.2
4.45
4.7
4.95
5.2
E (V)
0
0.1
0.5
0.4
0.3
0.3
0.4
0.5
0.1
0
Scan Rate=0.015mV/s
CE, RE=Li

Figure 7

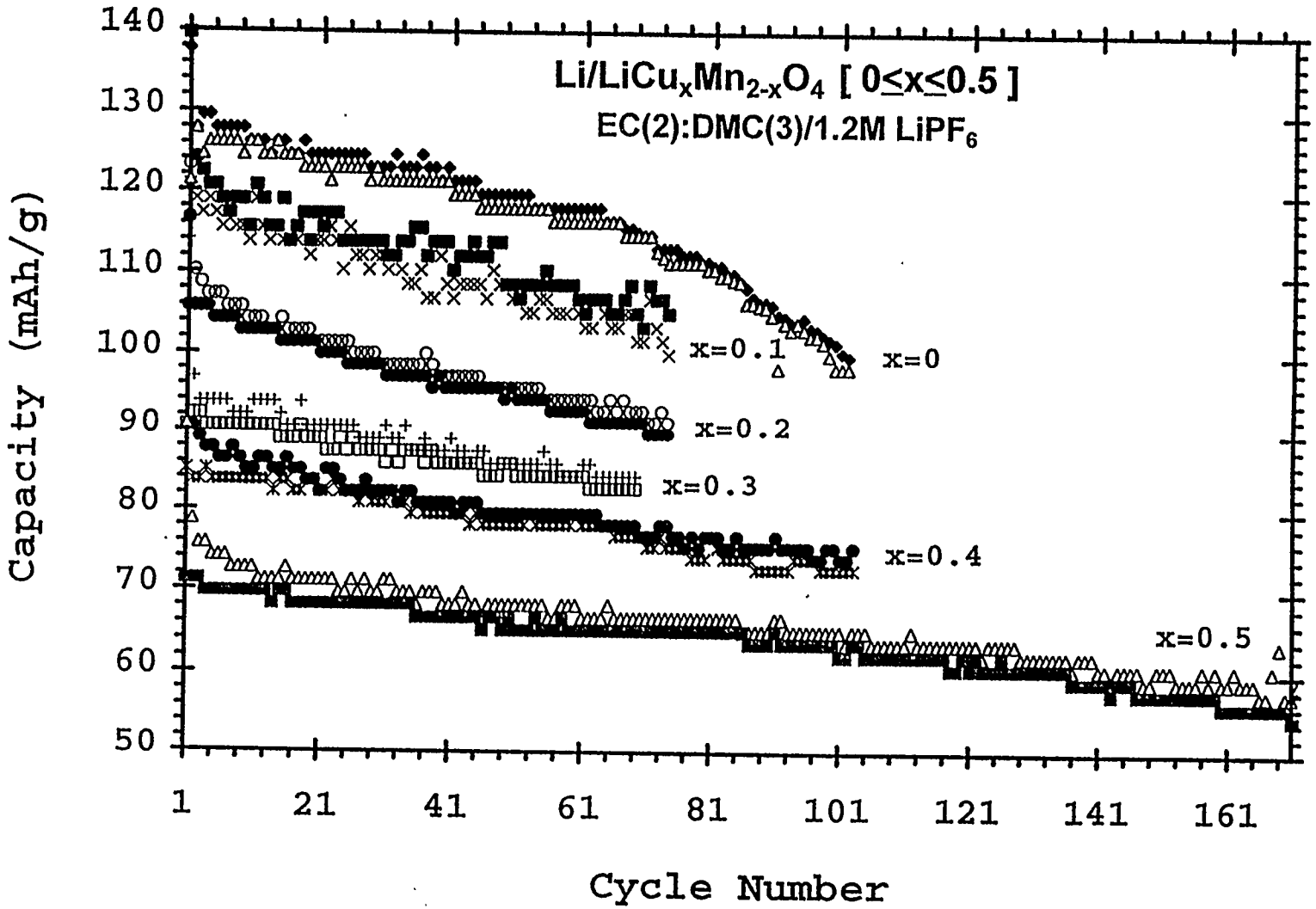
Li/LiCu$_x$Mn$_{2-x}$O$_4$ [0≤x≤0.5]
EC(2):DMC(3)/1.2M LiPF$_6$
x=0
x=0.1
x=0.2
x=0.3
x=0.4
x=0.5
Capacity (mAh/g)
Cycle Number
140
130
120
110
100
90
80
70
60
50
1
21
41
61
81
101
121
141
161

Figure 8

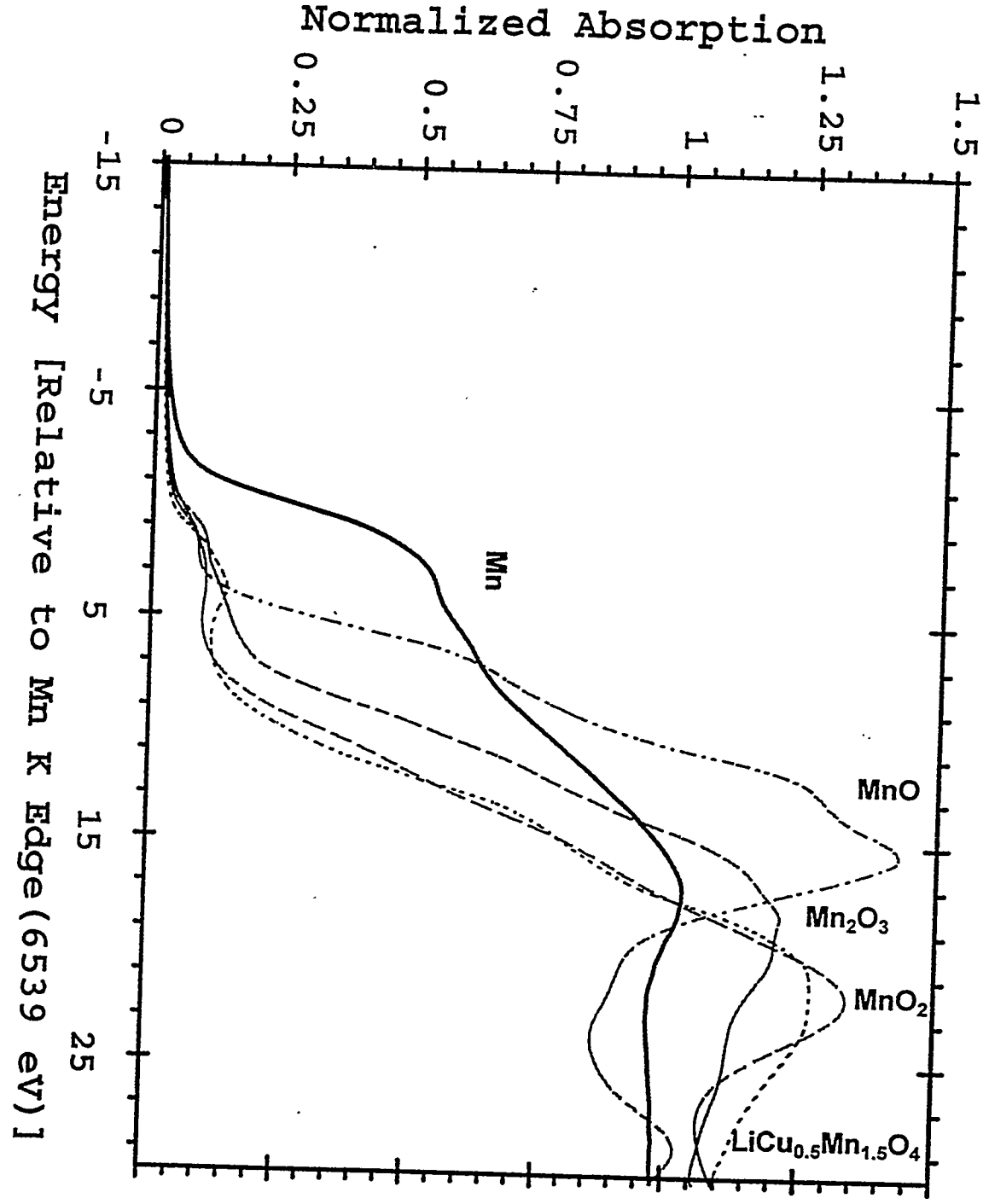
Normalized Absorption
0
0.25
0.5
0.75
1
1.25
1.5
Energy [Relative to Mn K Edge (6539 eV)]
-15
-5
5
15
25
Mn
MnO
Mn_2O_3
MnO_2
$LiCu_{0.5}Mn_{1.5}O_4$

Figure 9

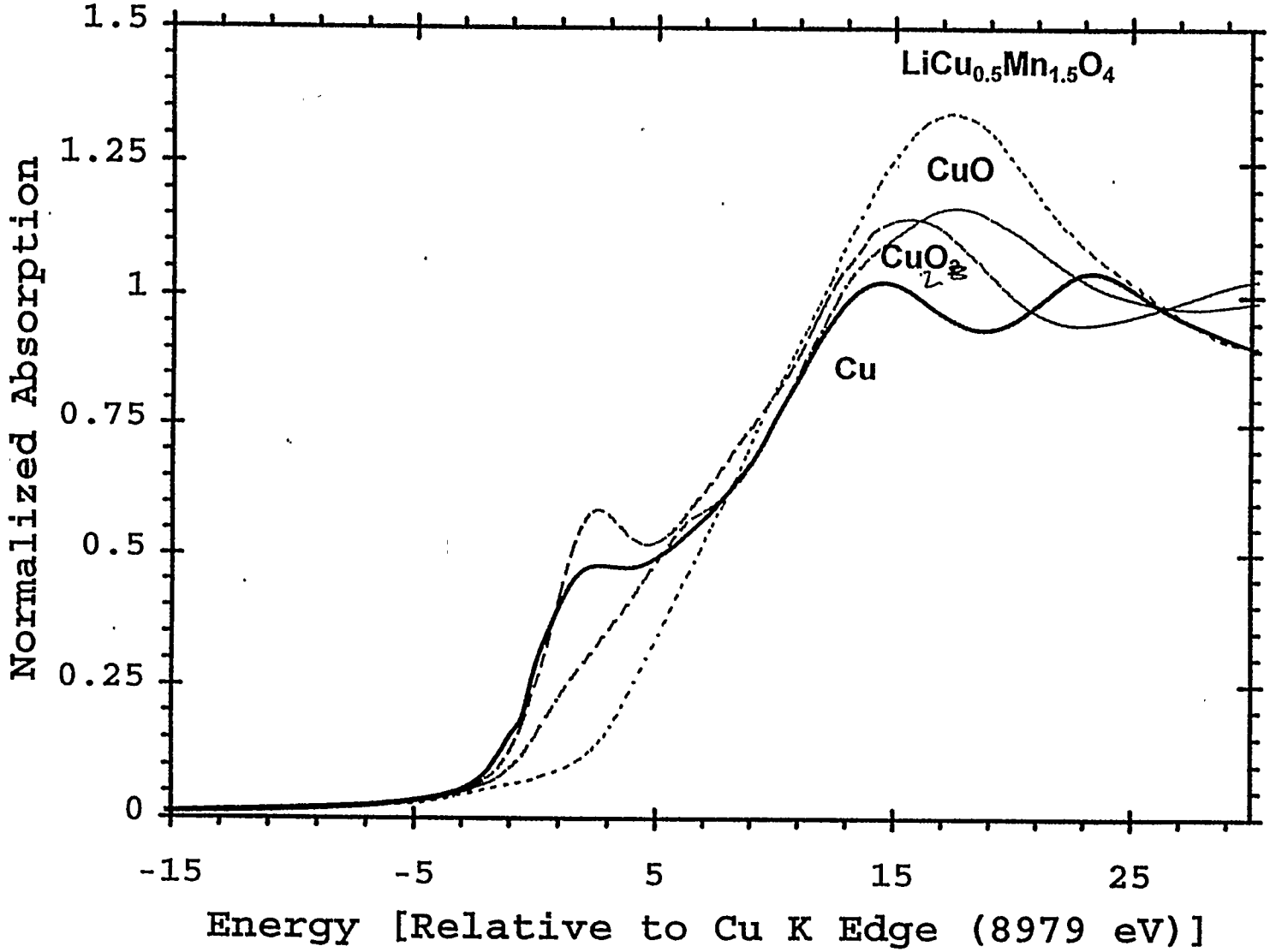
1.5
1.25
1
0.75
0.5
0.25
0
Normalized Absorption
LiCu0.5Mn1.5O4
CuO
CuO2
Cu
-15
-5
5
15
25
Energy [Relative to Cu K Edge (8979 eV)]

Figure 10

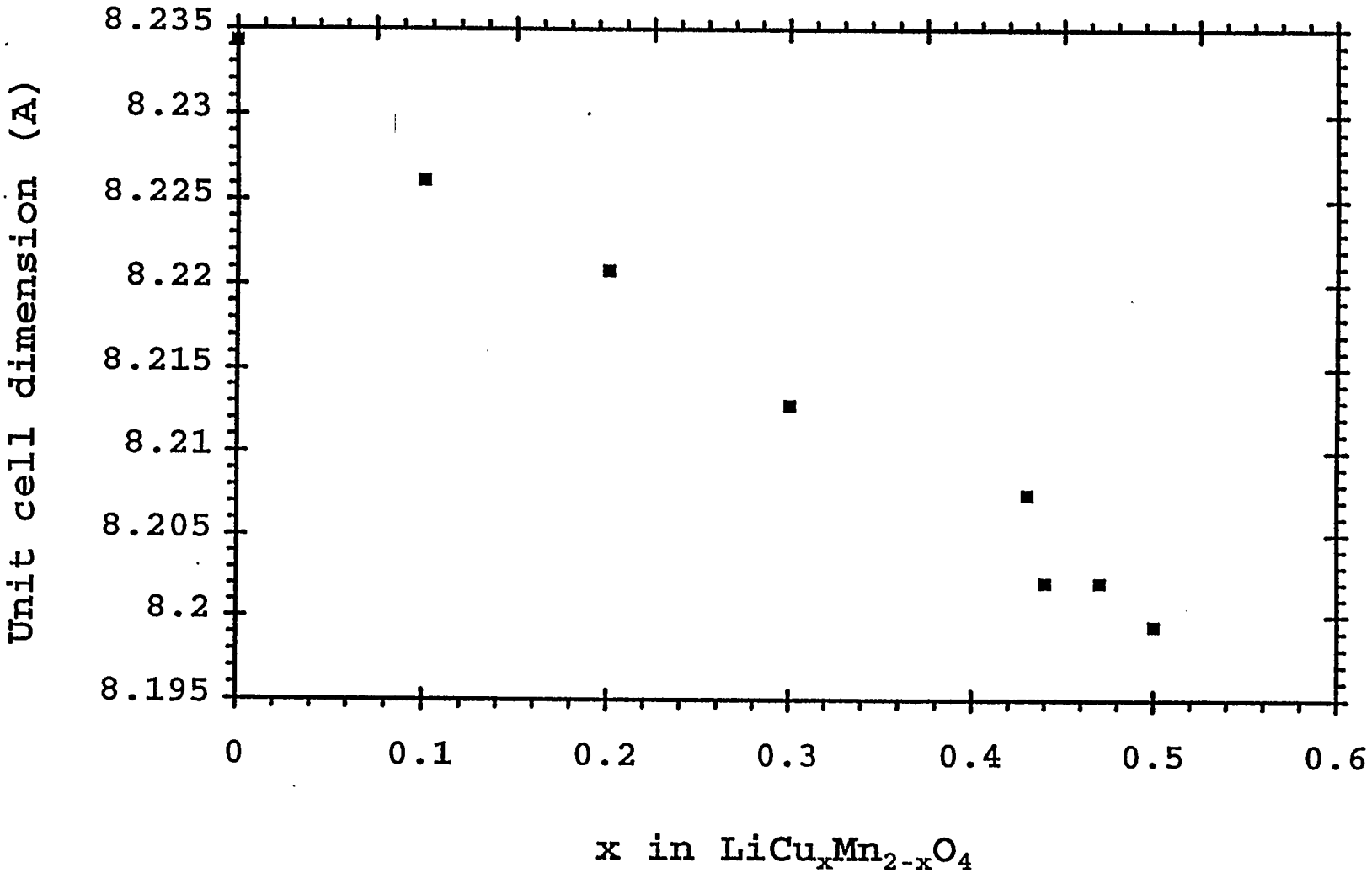
Unit cell dimension (A)
8.235
8.23
8.225
8.22
8.215
8.21
8.205
8.2
8.195
0
0.1
0.2
0.3
0.4
0.5
0.6
x in LiCu$_x$Mn$_{2-x}$O$_4$

Figure 11

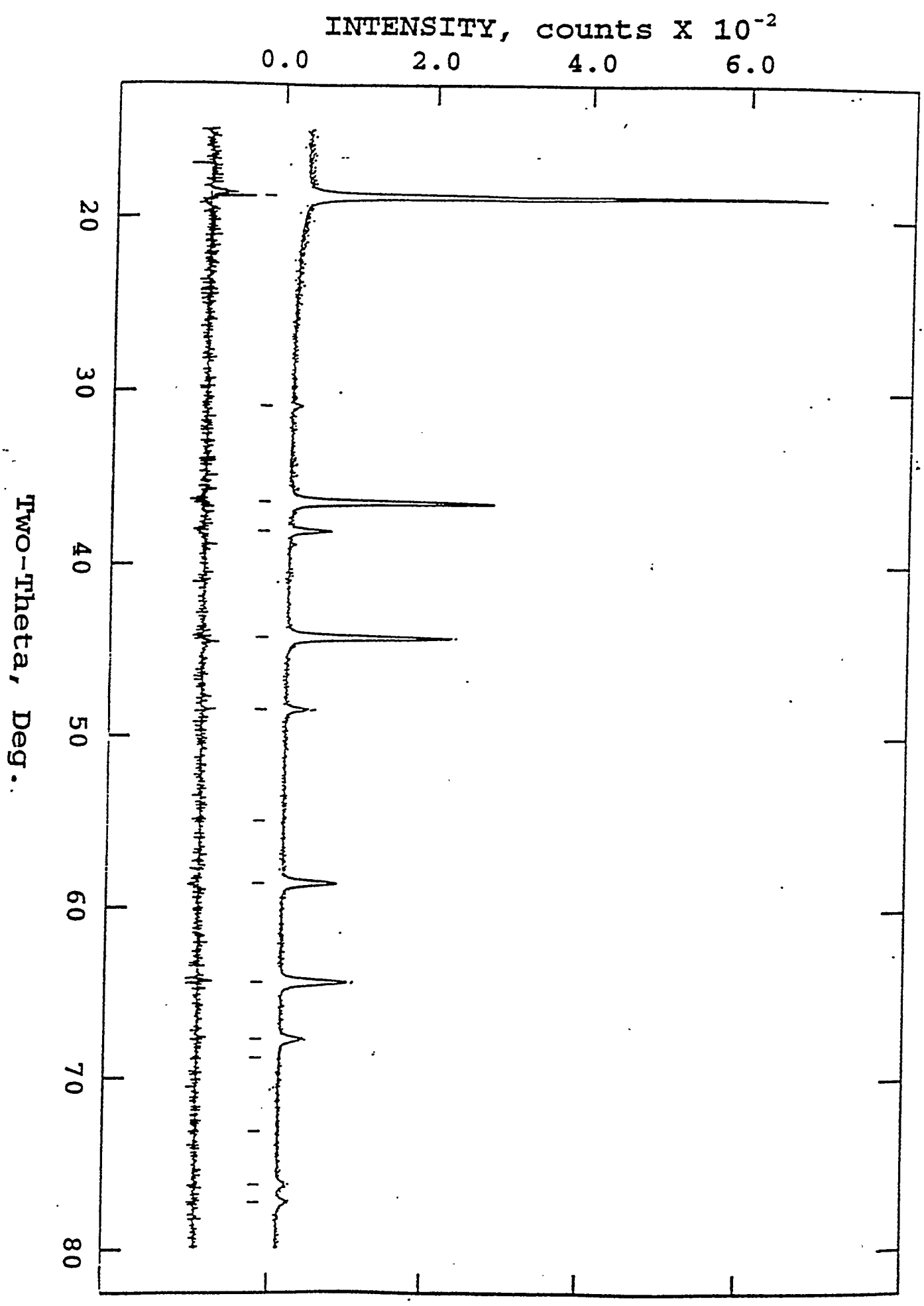
INTENSITY, counts X 10^{-2}
0.0
2.0
4.0
6.0
20
30
40
50
60
70
80
Two-Theta, Deg.

a

b

c

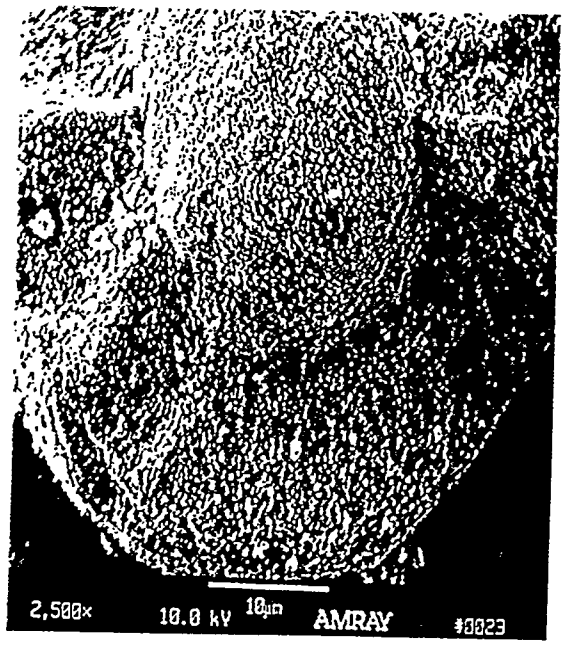

d

Figure 13

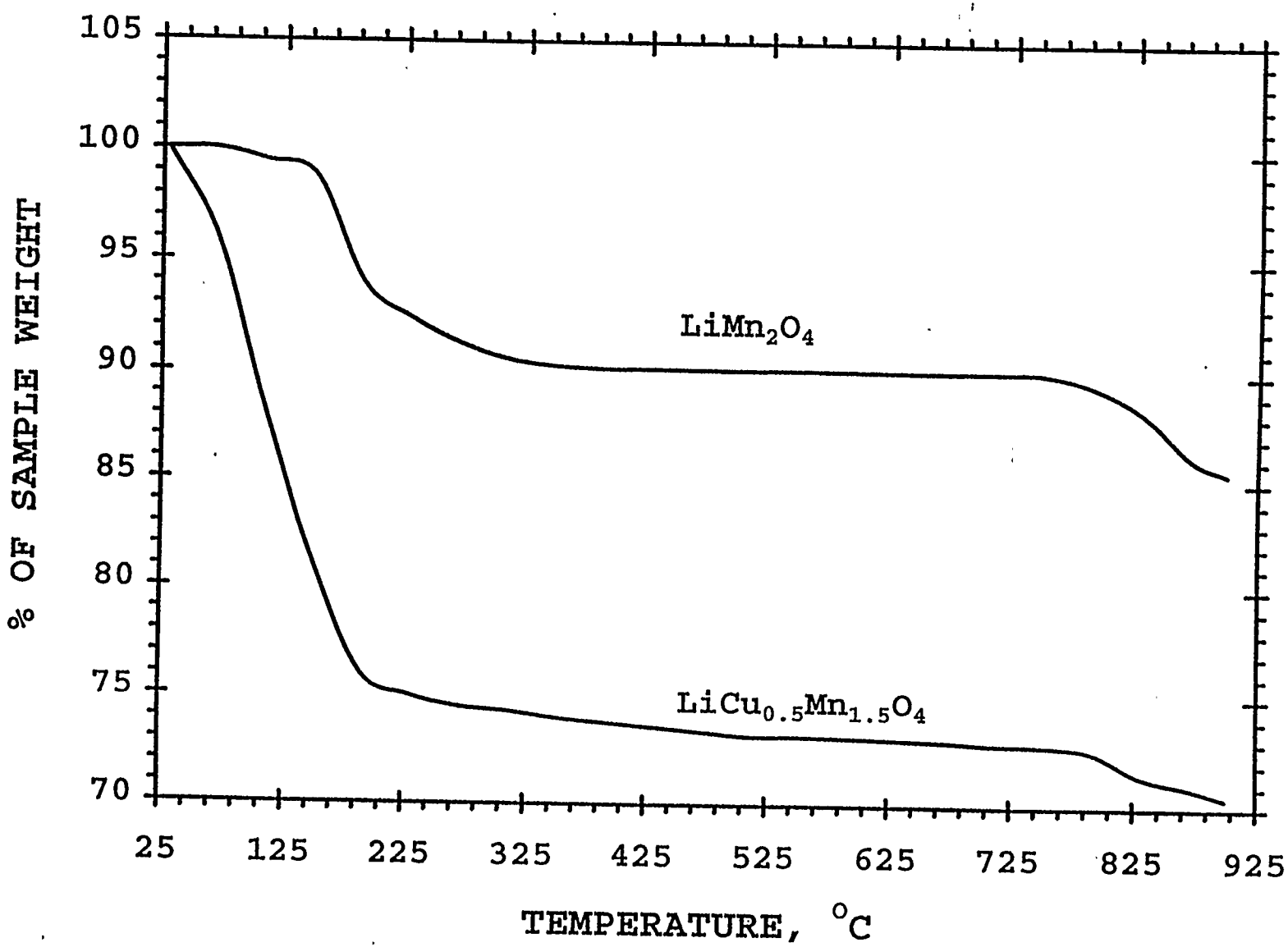
105
100
95
90
85
80
75
70
% OF SAMPLE WEIGHT
LiMn2O4
LiCu0.5Mn1.5O4
25
125
225
325
425
525
625
725
825
925
TEMPERATURE, °C

Figure 14